A Novel Approach to Simulate and Evaluate Submerged-Entry Nozzle Clogging Evolution Using the Full-Scale Physical Twin of a Continuous Casting Mold



Authors

Jackie Leung (top left), Senior Researcher — Primary Processing, ArcelorMittal Global R&D Hamilton, Hamilton, Ont., Canada, and Ph.D. Candidate, Department of Mechanical & Industrial Engineering, University of Toronto, Toronto, Ont., Canada
jackie.leung@arcelormittal.com

Donghui Li (top right), Senior Research Associate, Department of Materials Science & Engineering, University of Toronto, Toronto, Ont., Canada
donghui.li@utoronto.ca

Joydeep Sengupta (bottom), Principal Scientist (Primary Processes) ArcelorMittal Global R&D Hamilton, Hamilton, Ont., Canada
joydeep.sengupta@arcelormittal.com

Markus Bussmann, Department of Mechanical & Industrial Engineering, University of Toronto, Toronto, Ont., Canada

Submerged-entry nozzle (SEN) clogging during continuous casting is a well-known but not well-understood phenomenon, impacting steelmaking productivity and quality. Physical water modeling provides insight on mold flow, but prior studies including SEN clogging have used simplified approaches. The true shape of SEN clogging is complex, and its impact on mold flow may not be reflected during simulations. Additionally, SEN clogging formation is cumulative, but it can only be observed after the SEN's removal from the caster. In this article, realistically clogged SENs were replicated with enhancements and installed in a physical twin to study the impact on mold flow.

In a steelmaking continuous slab caster (Fig. 1a), liquid steel is transferred from the ladle into the tundish. Liquid steel then flows through the submerged-entry nozzle (SEN) and into the mold where steel solidification initiates and continues along the length of the continuous casting (CC) machine. The strand is torch cut and a slab is produced which will be rolled into a coil and sent to customers to be formed into products such as automotive parts and packaging such as tin cans (Fig. 1b).

Non-metallic inclusions, inherent to the steelmaking process, contribute to clogging of the refractory flow control components (Fig. 2a). Clogging detrimentally impacts mold fluid flow and potentially results in slab defects. A countermeasure to reduce clogging is to inject argon gas through these components. However, the addition of gas results in complex bubbly flow inside the mold.

Physical water modeling of the CC process has been used for decades to evaluate mold flow.[1] To simulate mold flow patterns generated by

Figure 1

Simplified schematic of slab continuous casting (CC) process (a);[5] Subsequent CC outputs: Slabs[6] → Coils[7] → Flat carbon steel products (e.g., tin cans[8] and automotive parts[9]) (b).

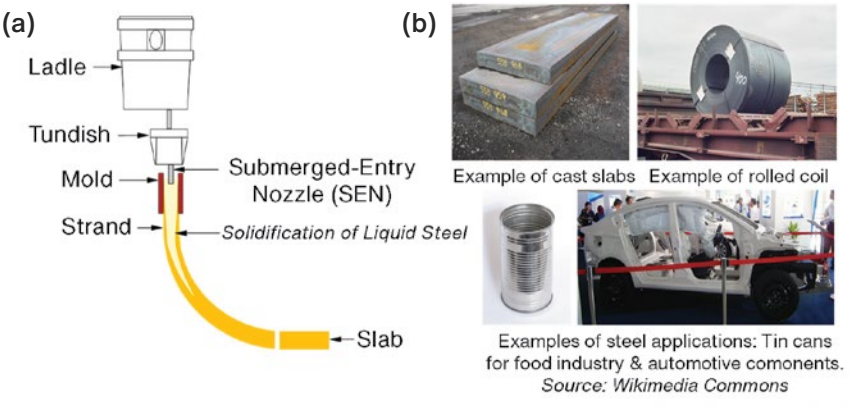

clogged SENs, at least one port of the SEN would be partially obstructed.[2–3] This has been a simplified approach to simulate SEN clogging in physical modeling. However, clogging does not only occur at the SEN port, but also along the interior surface (bore) of the SEN with its surface shape being very complex. Furthermore, clogging is an evolutive process and its impact on mold flow changes throughout the life of the SEN. In this report, four SENs, with varying levels of realistic clogging, were installed in a CC mold water model. A fifth SEN with no clogging was also tested as a baseline case. Mold flow generated by each clogged SEN was evaluated using sensors that measure fluid flow and compared to the baseline case.

Physical Twin

The physical twin (full-scale water model of a CC mold) is located at the University of Toronto (UofT) (Fig. 2b).[1,4] Walls of the mold are made of transparent acrylic to directly observe the flow of water. Air can be injected into the water through the stopper rod to simulate argon injection into liquid steel (Fig. 2c). Although the physical twin can be equipped with refractory-based SENs or stopper rods from the plant, 3D-printed versions were fabricated by the Additive Manufacturing Innovation Centre (AMIC) at Mohawk College in Hamilton, Ont., Canada.

Sensor Instrumentation

Fig. 3 shows the position of the sensors installed in the physical twin.[1] Sensors nearest to the mold narrow face walls are designated left-left (LL) and right-right (RR). Sensors nearest to the SEN are designated left-quarter (LQ) and right-quarter (RQ). All sensors were connected to a data acquisition device to record data for 60 second at a sampling rate of 10 × /second.

Four impeller anemometers provide continuous measurement of water velocity. They are positioned at the $^1/_3$- and $^1/_6$-mold width positions and submerged ~100 mm below the water level to measure submeniscus velocity along the x-axis (mold width direction). Four ultrasonic level sensors (ULSs) provide continuous measurement of distance from the sensor head to the water surface. They are positioned at the $^1/_4$-mold width positions (LQ and RQ) and 2 inches from the mold narrow face (NF) walls (LL and RR). The ULSs are positioned ~130 mm above water level. In this report, mold level is expressed as the distance between the water level and a fixed reference position (~130 mm from the sensor head) calculated using Eq. 1:

$$Mold\ Level = Distance_{(Sensor-Reference)} - Distance_{(Sensor-Water\ Level)} \quad \text{(Eq. 1)}$$

The mold level is then used to calculate standing wave height using Eq. 2:

$$Standing\ Wave\ Height = Mold\ Level_{NF} - Mold\ Level_{(1/4-mold\ width)} \quad \text{(Eq. 2)}$$

Figure 2

Simplified schematic of CC process in tundish and mold (a);[10] Physical twin (full-scale water model of a CC mold) at University of Toronto (b); Schematic of air injection into physical twin through stopper rod and submerged-entry nozzle (SEN) 3D-printed by the Additive Manufacturing Innovation Centre (AMIC) (c).

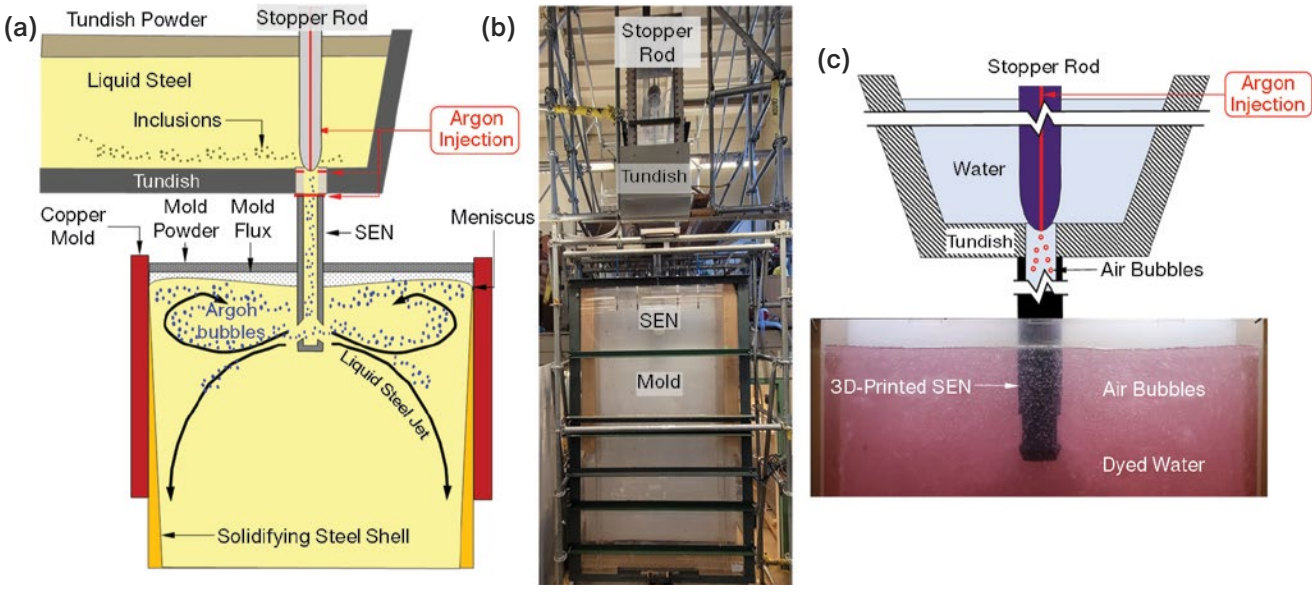

Figure 3

Impeller anemometers and ultrasonic level sensors (ULSs) installed in the physical twin to measure submeniscus velocity and mold level, respectively. Sensor designations: LL: left-left; LQ: left-quarter; RQ: right-quarter; RR: right-right.[1]

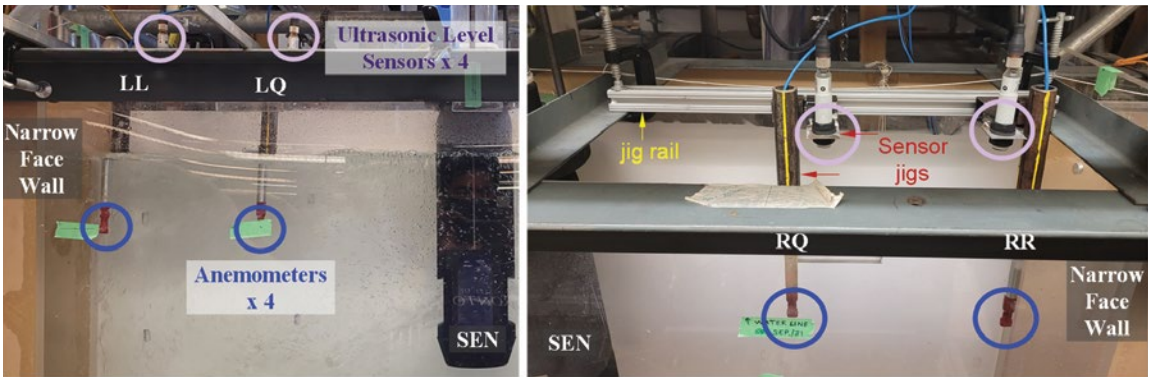

Figure 4

CAD model cross-section of clogged SEN tested in physical twin exhibiting clogged port on left and non-clogged port on right (a); CAD images of 3D-printed SENs (clogged side view) with progressively increasing levels of port clogging (clogging factor (CF)) (b).

Mass Reduction	0%	10%	15%	20%	25%	100%
SEN Clogging	100%	90%	85%	80%	75%	0%
SEN ID	N/A	CF90	CF85	CF80	CF75	CF0

The SENs used in this study were generated using computer-aided design (CAD) software (Fig. 4). Clogging was digitally added to the ports and bore of an SEN with hypothetical design specifications. The design specifications of this hypothetical SEN with no clogging are listed in Table 1. Clogging was added such that one SEN port was very clogged and another port was not clogged. A formation of clog material, bridging from front to back of the SEN, was also added (see CF100). The clog formation was digitally reduced evenly in 5% increments and reprinted to evaluate the evolution of SEN clogging on mold flow. In this study, four SENs with varying levels

Table 1

SEN-CF0 (No Clogging Baseline) Design Specifications

SEN ID	Port shape	Port angle	Well depth	Bore diameter
SEN-CF0	Square	–15°	0 mm	76.2 mm

of clogging factor (CF75, CF80, CF85 and CF90) were evaluated and compared to original (hypothetical) SEN, having no clogging, as the baseline case (CF0).

Each SEN was installed in the physical twin to simulate mold flow under certain casting parameters (Table 2). After setting the correct water and air flowrates and allowing enough time for the mold flow pattern to stabilize, the sensors were activated to record measurements.

Results

Mold Flow Visualization by Dye Injection

Fig. 5 shows dye injection tests conducted during experiments CF0, CF75 and CF90 to quickly visualize mold flow patterns. The SENs were installed so that the clogged port is on the left and the non-clogged port is on the right. The baseline case with no clogging shows a symmetric double-roll mold flow pattern (Fig. 5a). Conversely, experiments with CF75 and CF90, where the left SEN port is clogged, exhibited a stronger double roll on the right (non-clogged) side (Fig. 5b and 5c).

Submeniscus Velocity

Submeniscus velocity measurements are consistent with dye injection results. For the sake of brevity, the unaveraged sensor data for only CF90 and CF0 are shown (Figs. 6 and 7, respectively) with all cases summarized in Fig. 8 and Table 3. The asymmetry of mold flow is clear

Table 2

Physical Twin Experiment Parameters. Note: Air injection and simulated caster argon gas injection rates are based on modified Froude Number.[1,11]

Mold width	Mold thickness	Water flowrate	Simulated cast speed	Air injection rate	Simulated argon gas injection rate
1,250 mm	220 mm	~380 L/min	1.4 m/min	6 L/min	5.5 L/min

Figure 5

Physical twin simulations with dye injection using SEN-CF (a), SEN-CF75 (b) and SEN-CF90 (c).

(a) (b) (c)

Figure 6

SEN-CF90 submeniscus velocity measured on left (clogged) (a) and right (non-clogged) (b) sides of SEN.

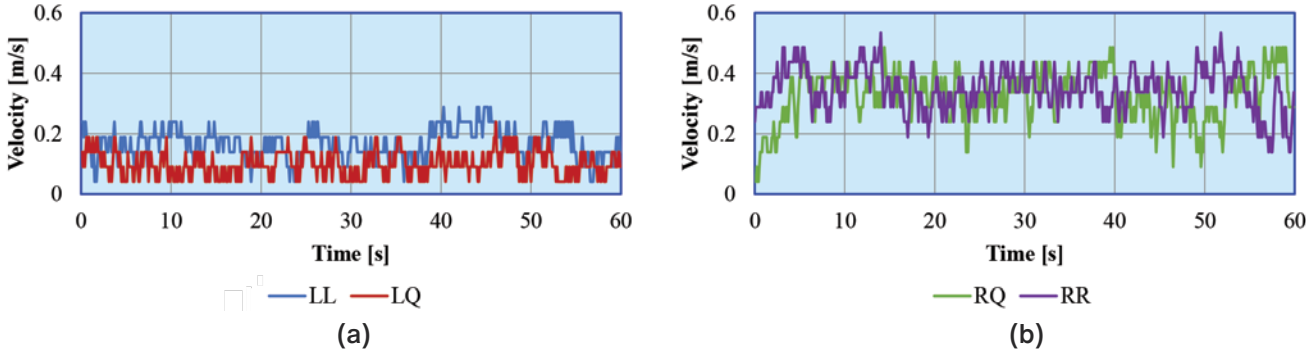

Figure 7

SEN-CF0 (no clogging) submeniscus velocity measured on left (a) and right (b) sides of SEN.

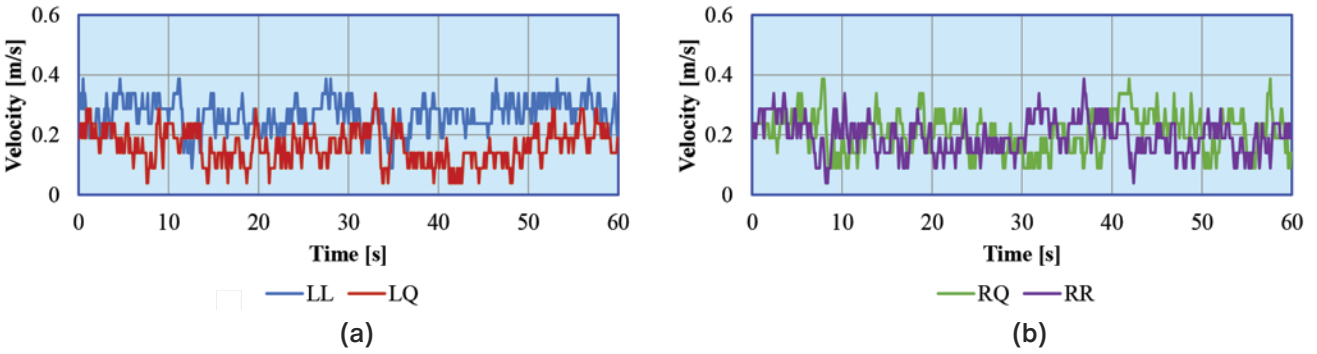

in the case of CF90, with high velocities on the right (non-clogged) side and low velocities on the left (clogged) side of the SEN (Fig. 6). This is in contrast with SEN-CF0 (Fig. 7), where velocity is relatively symmetric. It is also interesting to note in CF90 that while the right side has higher velocities than baseline, which is expected, the left side exhibits lower velocity than baseline, indicating less active mold flow.

Fig. 8 compares average submeniscus velocity for all cases. Asymmetric submeniscus velocity between right and left sides is present for all clogged SENs. Velocity progressively increases with increasing CF on the right side. Conversely, velocity on the left side was relatively consistent or even arguably lower with increasing CF.

Table 3 compares average submeniscus velocity for all cases, the change from the baseline case, and mold flow asymmetry (RR vs. LL results). Mold flow asymmetry in the baseline case was 24% (difference of 0.06 m/second). This was likely due in part to stopper rod misalignment.[11] Taking into account the effect of stopper rod misalignment in the baseline case with no clogging, there are still substantial increases in velocity and mold flow asymmetry with SEN clogging. Velocities on the non-clogged side increase with CF up to 80% compared to the clogged side. Submeniscus velocity and/or mold flow asymmetry do not increase or decrease at a constant rate with CF. This is reflective of the complex nature of SEN clogging and mold flow.

SEN Port Jet Velocity

The anemometers were repositioned and manually held to measure SEN port jet velocity (Fig. 9a). The anemometers were angled to be in line with the direction of jet velocity (Fig. 9b) but were difficult to hold in place due to the increased water velocity. It was also observed that bubbly flow was not consistent along the height of the SEN ports (i.e., more bubbly flow was present at the upper half of the ports). Hence, only the maximum jet velocity was recorded (Table 4).

Water velocity at the SEN port jet is an order of magnitude higher than at the submeniscus location. Jet velocity increased at both ports with increasing CF up to 73%. Mold flow asymmetry in the baseline case is –6%, which is likely due to stopper rod misalignment. For CF90, port velocity is higher on the unclogged side, which is consistent with the submeniscus velocity measurements.

Figure 8

Average submeniscus velocity for all cases of CF on left (clogged) (a) and right (non-clogged) (b) sides of SEN. Note: Error bars are 1 standard deviation.

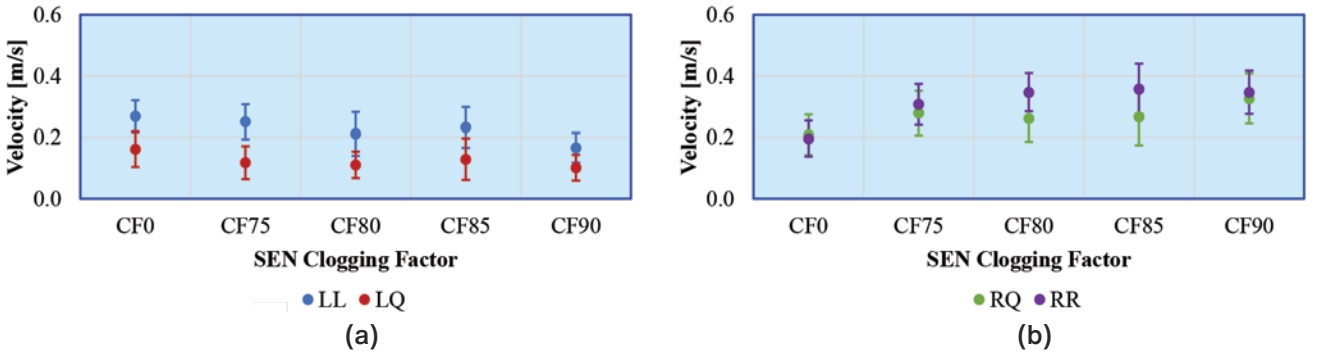

Table 3

Evaluation of Average Submeniscus Velocity and Mold Flow Asymmetry (Δ RR vs. LL)

	LL		LQ		RQ		RR		
SEN ID	[m/s]	Δ from CF0	[m/s]	Δ from CF0	[m/s]	Δ from CF0	[m/s]	Δ from CF0	Δ RR vs. LL
CF0	0.27	—	0.16	—	0.21	—	0.20	—	-26%
CF75	0.25	-7%	0.12	-25%	0.28	+33%	0.31	+55%	+24%
CF80	0.21	-22%	0.11	-31%	0.26	+24%	0.35	+75%	+67%
CF85	0.23	-15%	0.13	-19%	0.27	+29%	0.36	+80%	+57%
CF90	0.17	-37%	0.10	-38%	0.33	+57%	0.35	+75%	+106%

Table 4

Evaluation of Maximum SEN Port Jet Velocity (Measured Manually) and Mold Flow Asymmetry

	Left (clogged) side		Right (non-clogged) side		
SEN ID	[m/s]	Δ from CF0	[m/s]	Δ from CF0	Δ Right vs. left
CF0	1.6	—	1.5	—	-6%
CF75	2.1	+31%	2.1	+40%	0%
CF90	2.3	+44%	2.6	+73%	+13%

However, for CF75, port jet velocities are nearly the same. The maximum port jet velocity does not reflect the varying velocities exiting the SEN ports. Velocities can be far lower along the height of the port. Hence, the overall volumetric flowrates of both ports can still differ. A controlled study with longer duration measurements with the sensors fixed in place near the SEN ports is planned as future work.

Mold Level

Figs. 10 and 11 show mold level measurements for CF90 and CF0, respectively. Asymmetric mold level is very

Figure 9

Schematic of anemometer position for SEN port jet velocity measurement (a) and measurement taken during physical twin experiment (b).

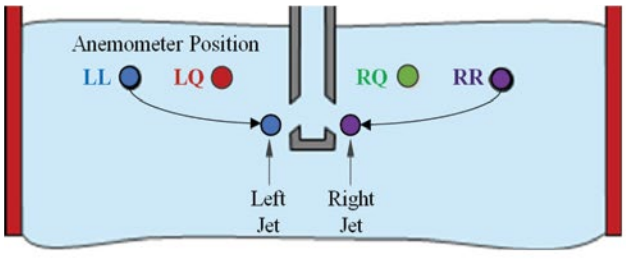

(a)

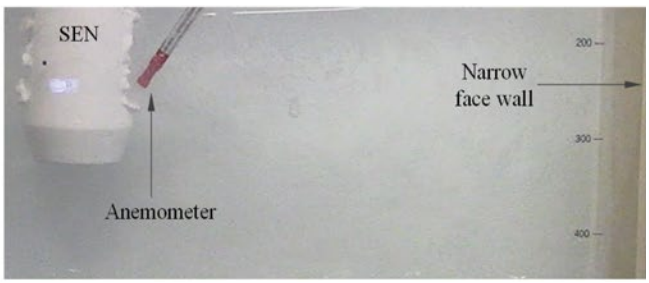

(b)

Figure 10

SEN-CF90 mold levels measured on left (clogged) (a) and right (non-clogged) (b) sides of SEN.

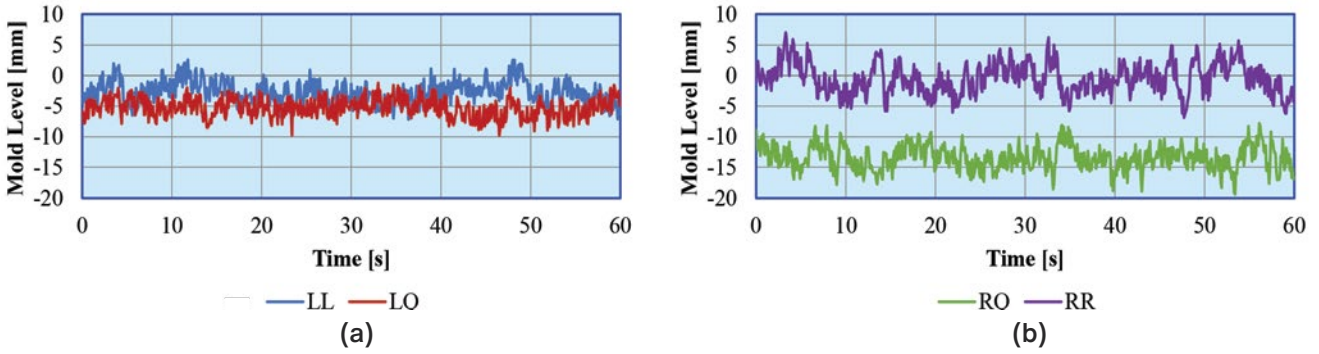

Figure 11

SEN-CF0 (no clogging) mold levels measured on left (a) and right (b) sides of SEN.

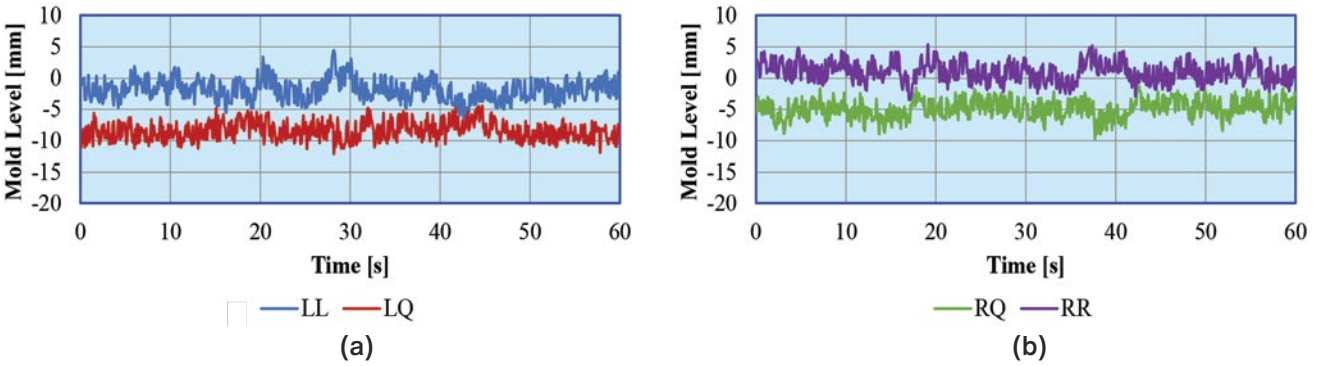

Figure 12

Average mold level for all cases of CF on a left (clogged) (a) and right (non-clogged) (b) sides of SEN. Note: Error bars are 1 standard deviation.

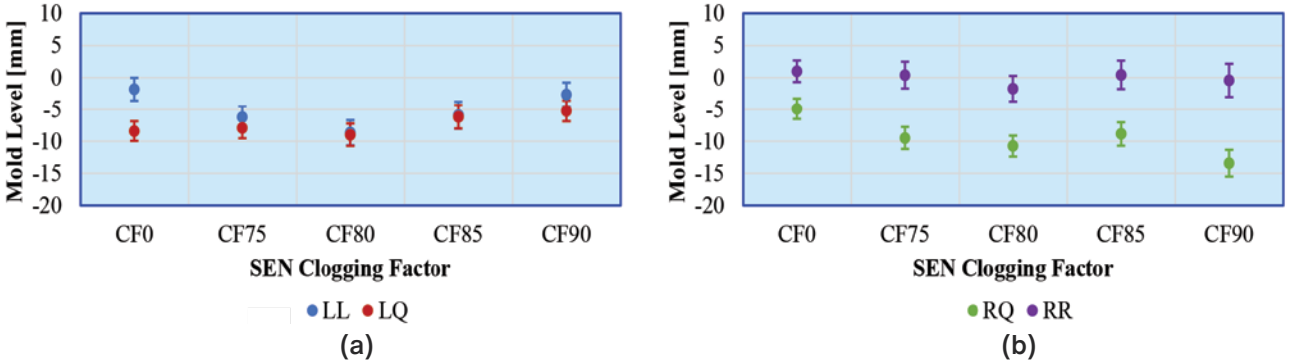

Table 5

Evaluation of Mold Level Fluctuations Based on ULS Standard Deviation and Mold Flow Asymmetry

	LL		LQ		RQ		RR		
SEN ID	[mm]	Δ from CF0	[mm]	Δ from CF0	[mm]	Δ from CF0	[mm]	Δ from CF0	Δ RR vs. LL
CF0	1.80	—	1.55	—	1.59	—	1.68	—	-7%
CF75	1.69	-6%	1.65	+6%	1.72	+8%	2.10	+25%	+24%
CF80	1.99	+11%	1.74	+12%	1.63	+3%	2.01	+20%	+1%
CF85	2.11	+17%	1.80	+16%	1.83	+15%	2.22	+32%	+5%
CF90	1.89	+5%	1.65	+6%	2.08	+31%	2.60	+55%	+38%

clear in the case of CF90, with higher and lower mold level positions on the right side of the SEN compared to the left. This difference in mold level is reflective of a standing wave, which will be discussed in the next section. The right side of CF90 exhibits more mold level fluctuations than the left side, and also more than the fluctuations observed in the baseline case.

Fig. 12 compares average mold levels for all cases. Asymmetric mold level is present in all cases of CF. Mold level positions on the right side move farther apart between the RR and RQ locations, whereas on the left side, mold level positions are closer together, indicating less active mold flow.

Table 5 shows mold level fluctuations, expressed as standard deviation, for all cases, the change from the baseline case, and mold flow asymmetry (RR vs. LL results). Mold level fluctuations exhibit an overall increasing trend with CF, particularly on the right side. Furthermore, asymmetry of mold levels between RR and LL ULSs increases from -7% in the baseline case, to 38% in CF90.

Standing Wave

Fig. 13 and 14 compare standing wave formation in CF90 and CF0, respectively. The standing wave generated on the right (non-clogged) side of the SEN is apparent (Fig. 13b), whereas the standing wave on the left side is comparable to the baseline case. It is also interesting to note that standing wave height is not constant, but rather dynamic, as the range of standing wave height fluctuates between 4 and 23 mm.

Fig. 15 compares average standing wave height for all cases. Standing wave height generally increases on the right side and decreases or arguably plateaus on the left side with increasing CF. However, it is unclear if standing wave formation plateaus on the right side. Additional experiments, conducted at higher and lower cast speeds, and their influence on standing wave height are planned as future work.

Figure 13

SEN-CF90 standing wave height on left (clogged) (a) and right (non-clogged) (b) sides of SEN.

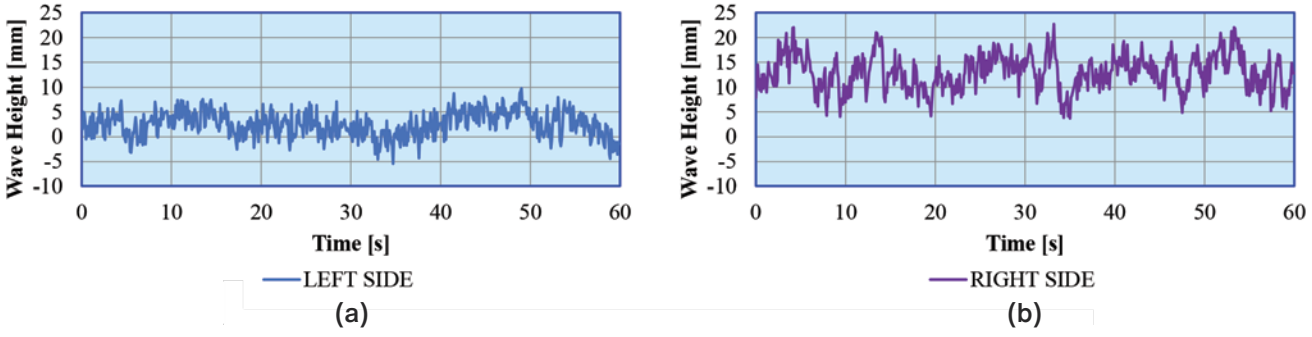

Figure 14

SEN-CF0 (no clogging) standing wave height on left (a) and right (b) sides of SEN.

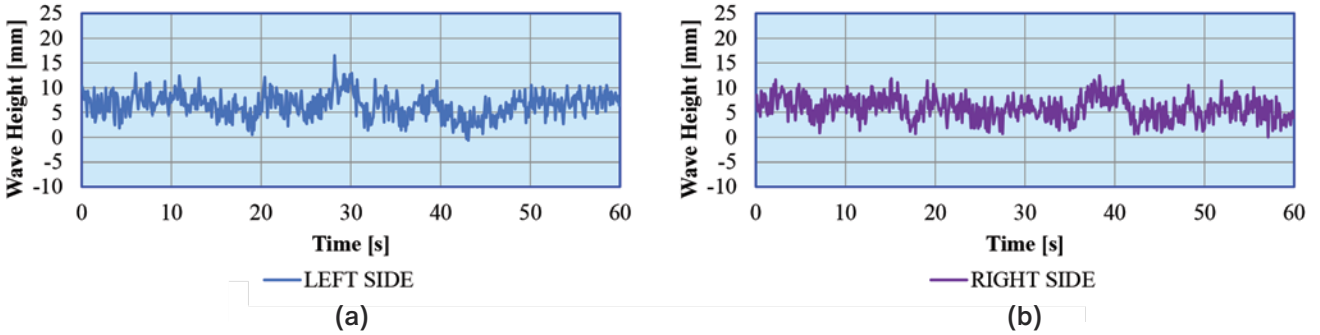

Figure 15

Average standing wave height for all cases of CF on left (clogged) (a) and right (non-clogged) (b) sides of SEN. Note: Error bars are 1 standard deviation.

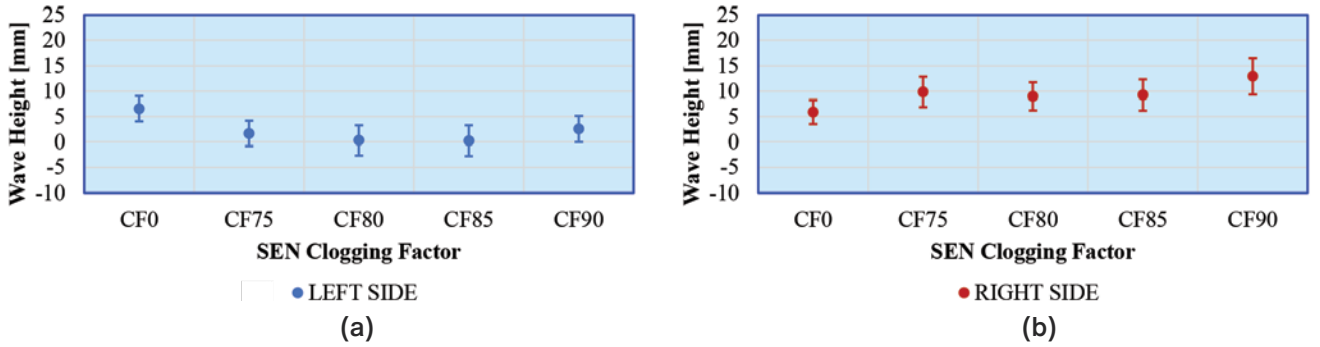

Table 6

Evaluation of Standing Wave Height and Mold Flow Asymmetry

	Left (clogged) side		Right (non-clogged) side		
SEN ID	[mm]	Ratio to CF0	[mm]	Ratio to CF0	Right/ left
CF0	6.6	—	5.9	—	0.9x
CF75	1.7	0.3x	9.9	1.7x	6x
CF80	0.3	0.05x	9.0	1.5x	30x
CF85	0.3	0.05x	9.3	1.6x	31x
CF90	2.6	0.4x	13.0	2.2x	5x

Table 6 summarizes standing wave height for all cases, the change from the baseline case, and mold flow asymmetry (Right vs. Left side results). Standing wave height increases 2x on the right side and reduces to <1x on the left side compared to the baseline case. Furthermore, the asymmetry of standing wave height from right side to left side increases from 1x in the baseline case, up to 31x for CF85.

Summary and Conclusions

Four SENs were 3D printed with their right ports clogged and lefts ports not clogged. The four SENs had incrementally increasing levels of clogging factor (CF75, CF80, CF85 and CF90). Some clogged

SENs had a bridge formation of clog material within the bore of the SEN. The SENs were installed in the physical twin to study the impact of SEN clogging evolution on mold flow behavior. An SEN with hypothetical design specifications and no clogging was also tested as a baseline (CF0). The following conclusions are drawn:

1. Asymmetric SEN clogging results in increased mold flow activity on the right (non-clogged) side compared to the baseline case based on the following findings:
   a. Stronger double roll on the right (non-clogged) side visualized by dye injection tests.
   b. Increase in submeniscus velocity, as high as 80% (from 0.20 to 0.36 m/second).
   c. Increase in SEN port jet velocity, as high as 73% (from 1.5 to 2.6 m/second).
   d. Increase in mold level fluctuations, expressed as standard deviation of water level position, as high as 55% (from 1.68 to 2.60 mm).
   e. Increase in standing wave height, as high as 2.2x (from 5.9 to 13.0 mm).
2. Asymmetric SEN clogging results in decreased, similar or increased mold flow activity on the left (clogged) side compared to the baseline case. However, in the case of increased mold flow activity, the increase is far less than the right side.
   a. Similar double roll on the left (clogged) visualized by dye injection tests.
   b. Decrease in submeniscus velocity, as much as –38% (from 0.16 to 0.10 m/second).
   c. Increase in SEN port jet velocity, as high as 44% (from 1.6 to 2.3 m/second).
   d. Change in mold level fluctuations, ranging from –6% to +17% (from 1.80 to 1.69–2.11 mm).
   e. Decrease in standing wave height, as low as 0.05x (from 6.6 to 0.3 mm).
3. Asymmetric SEN clogging results in mold flow asymmetry, expressed as the difference between the right and left sensors, based on the following findings:
   a. Increased asymmetric submeniscus velocity, as high as 106% (0.35 vs. 0.17 m/second) in the case of CF90. Asymmetry in the baseline case was –26% (0.20 vs. 0.27 m/second), likely due to misalignment of the stopper rod.
   b. Increased asymmetric SEN port jet velocity, as high as 13% (2.6 vs. 2.3 m/second) in the case of CF90. Asymmetry in the baseline case was –6% (1.5 vs. 1.6 m/second).
   c. Increased asymmetric mold level fluctuations, as high as 38% (2.60 vs. 1.89 mm) in the case of CF90. Asymmetry in the baseline case was –7% (1.68 vs. 1.80 mm).
   d. Increased asymmetric standing wave height, as high as 31x in the case of CF85. Asymmetry in the baseline case was 0.9x (5.9 vs. 6.6 mm).
4. This work was based on only one case of clog formation where one SEN port was clogged, and another port was not clogged. Not all instances of SEN clogging are so asymmetric. SEN clog formation can evolve differently depending on many factors not included in this study.

Acknowledgments

The authors would like to thank their colleagues at ArcelorMittal Dofasco G.P., ArcelorMittal Global R&D Hamilton, the University of Toronto and the Additive Manufacturing Innovation Centre at Mohawk College for their support in this work.

Disclaimer

This article is available online at AIST.org for 30 days following publication.

References

1. J. Leung, S. Dinda et al., "Sensor Instrumentation and Advanced Imaging of the Full-Scale Physical Twin Mold for Digital Data Generation During Continuous Casting," *AISTech 2023 Conference Proceedings,* 2023, pp. 1194–1203.
2. Image attribution: Borvan53, CC BY-SA 3.0, via Wikimedia Commons, "Stack of slabs at the Florange steelshop (France, Moselle)," 20 February 2010, accessed 23 February 2023, https://commons.wikimedia.org/wiki/File:Slabs_stack.jpg.
3. Image attribution: Methem (M. Putkonen), Public domain, via Wikimedia Commons, "A Rolled Steel Coil (possibly by Rautaruukki) in the VR Freight Yard at the City of Oulu in Finland," June 2009, accessed 23 February 2023, https://commons.wikimedia.org/wiki/File:Rolled_coil_in_Oulu_Jun2009_001.jpg.

4. Image attribution: Sun Ladder, CC BY-SA 3.0, via Wikimedia Commons, “An Empty Tin Can,” 19 January 2009, https://commons.wikimedia.org/wiki/File:Empty_tin_can2009-01-19.jpg, accessed 23 February 2023.
5. Image attribution: Aero777, CC BY-SA 2.5 MY, via Wikimedia Commons, “Proton Prevé RESS (Reinforced Safety Structure),” March 1, 2014, accessed 23 February 2023, https://commons.wikimedia.org/wiki/File:Proton_Prev%C3%A9_RESS_(Reinforced_Safety_Structure)_(03).jpg.
6. P. Mishra, S.K. Ajmani et al., “Review Article on Physical and Numerical Modeling of SEN and Mould for Continuous Slab Casting,” *Int. J. of Eng. Sci. and Tech.,* Vol. 4, No. 5, 2012, pp. 2234–2243.
7. P.S. Srinivas, A. Singh et al., “Multiphase Vortex Flow Patterns in Slab Caster Mold: Experimental Study,” *ISIJ International,* 2017, Vol. 57, No. 9, pp. 1553–1562.
8. S-M. Cho, S-H. Kim et al., “Effect of Nozzle Clogging on Surface Flow and Vortex Formation in the Continuous Casting Mold,” *Iron & Steel Technology,* 2012, No. 7, pp. 85–95.
9. L. Zhang, Y. Wang and X. Zuo, “Flow Transport and Inclusion Motion in Steel Continuous-Casting Mold under Submerged Entry Nozzle Clogging Condition,” *Metallurgical and Materials Transactions B,* 2008, Vol. 39B, pp. 534–550.
10. B. Konar, D. Li and K. Chattopadhyay, “Demystifying the CC Mold at the University of Toronto: The First Full-Scale Mold Water Model in North American Academia,” *AISTech 2019 Conference Proceedings,* 2019, pp. 1331–1344.
11. J. Leung, S. Dinda and K. Chattopadhyay, “Enhancements to the Mould Water Model Physical Twin of a Continuous Steel Slab Caster for Machine Learning Development,” *Canadian Materials Science Conference 2022,* The Metallurgy and Materials Society of CIM, 2022.
12. A. Srivastava and K. Chattopadhyay, “Macroscopic Mechanistic Modeling for the Prediction of Mold Slag Exposure in a Continuous Casting Mold,” *Metallurgical and Materials Transactions B,* Vol. 53, No. 2, 2022, pp. 1018–1035. ✦

This paper was presented at AISTech 2024 — The Iron & Steel Technology Conference and Exposition, Columbus, Ohio, USA, and published in the AISTech 2024 Conference Proceedings.